JCTC Journal of Chemical Theory and Computation

Article

pubs.acs.org/JCTC

New Insight into the Topology of Excited States through Detachment/Attachment Density Matrices-Based Centroids of Charge

Thibaud Etienne,*[,†,‡,§] Xavier Assfeld,[†,‡] and Antonio Monari[†,‡]

[†]Université de Lorraine − Nancy, Théorie-Modélisation-Simulation, SRSMC, Boulevard des Aiguillettes, 54506 Vandoeuvre-lès-Nancy, France

[‡]CNRS, Théorie-Modélisation-Simulation, SRSMC, Boulevard des Aiguillettes, 54506 Vandoeuvre-lès-Nancy, France

[§]Unité de Chimie Physique Théorique et Structurale, Université de Namur, Rue de Bruxelles 61, 5000 Namur, Belgium

Supporting Information

ABSTRACT: In parallel with the derivation of a novel descriptor (ϕ_S) related to chromophores' electronic excited states topology, the present article emphasizes some congruence of significance between our ϕ_S index and formerly developed centroid-related indices. We especially point out the possibility to formally adapt a barycenter (centroid) approach to the use of detachment/attachment densities. While the reciprocity of the two approaches can be mathematically evidenced, we will show that some difficulties brought by the use of ground and excited states electron densities in direct space can be overcome by undertaking some operations on the Hilbert space-related detachment/attachment matrices. We further wish to point out the crucial case of some chromophores holding two electron-withdrawing groups symmetrically disposed in a rod-like structure. Finally, we will qualitatively highlight the quadratic-like relationship between the amount of displaced charge induced by light absorption and the ϕ_S index.

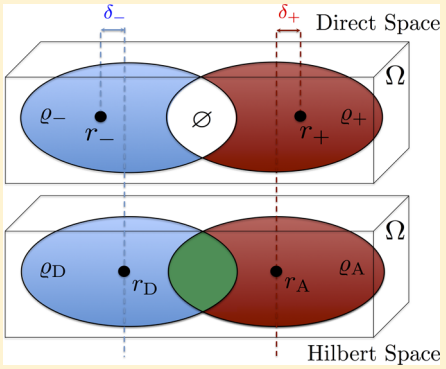

1. INTRODUCTION

Probing the potentiality of a chromophore to undergo a charge-transfer induced by light absorption constitutes an important achievement in the characterization of the dye's optical properties.[1−3] Together with the maximum absorption wavelength and the band shape, this information allows one to achieve a better understanding of the target compound's photoactivity. Hence, such knowledge can be crucial in a molecular design of new chromophores or during the rationalization of experimental data through theoretical calculations.[4−6]

Beyond this important issue, the outcome of such an analysis can provide an interestingly accurate and precise understanding of the physical nature of an excited state itself. Indeed, when the concern consists in building an original photoactive device, one wishes most often to obtain novel efficient chromophores that exhibit low-energy light absorption together with long-range charge-transfers.[7] This is true for light-energy conversion (DSSC), energy storage (photocatalysis), or emitting devices and materials. Actually, those excited state properties have a univocal relationship with the performances of the device itself.

While the sensitizer's transition energies can be computed with reliable quantum chemical methods, the quantitative estimation of the charge-transfer or valence character of a transition is more tricky. The quality of molecular design strategies highly relies on how fine and quantitative is the analysis of the nature of the excited states in terms of both their energy and the topology of electron density reorganization.

Such a need paves the way for conceiving new conceptual approaches to the quantification of electron density reorganization upon excitation.[8,9] For instance, one can evaluate the amount of charge displaced during light absorption using the location of the centroid of charge fluctuation.[10−13] This first so-called *barycenter* approach involves a preliminary operation consisting in the computation of the difference between excited and ground state electron densities in the direct (3D real) space. A distinction between negative and positive variations follows: The negative and positive values are actually representing "hole" and "particle" densities, respectively. The integration of these densities through all the space returns the amount of transferred charge. To obtain a simple index related to charge-transfer, the distance between the two centroids of those densities is calculated, as detailed in the Theoretical Background and Computational Details section.

Our new approach suggests the use of detachment/attachment densities,[14] which also physically depict the hole/particle generated by the electronic transition but with different theoretical foundations to calculate the centroid of charge.[15] In particular, the construction of these detachment/attachment densities requires a preliminary operation similar to the

Received: May 7, 2014
Published: July 23, 2014

barycenter approach, but this operation is here performed in the Hilbert space (i.e., in the canonical orbitals LCAO space) because the difference between excited and ground states density matrices is used as a first step. Furthermore, as we have recently shown,[16] assessing the overlap between detachment and attachment densities in the direct space through the dimensionless ϕ_S descriptor[16] further allows us to quantify the charge-transfer magnitude. Indeed, a transition with a high charge-transfer character will be characterized by a low ϕ_S value. Conversely, valence-type transitions have significantly higher values of ϕ_S.

As we will demonstrate, these two approaches have common points so that ground/excited states electron densities and detachment/attachment densities can therefore be invariably used for the assessment of the quantities involved in the barycenter approach, namely, the amount of transferred charge and intercentroid distances.

We will also explain and illustrate the fact that the interbarycenters distance values are different when calculated from direct space operations only or by simply computing detachment/attachment densities centroids.

Furthermore, the barycenter approach exhibits some difficulties in the case of rod-like molecules symmetrically holding electron-withdrawing groups, for which the intercentroid distance is systematically zero independently of the amount of transferred charge. We will show that such an issue can be eluded by the use of detachment/attachment densities and the ϕ_S descriptor.

The relation between the different descriptors is illustrated by extensive numerical tests performed on commonly used chromophores.

The details related to the molecular test set can be found in the Computational Strategy section. The barycenter-related indices as well as the ϕ_S descriptor computation in present survey consist of a time-dependent density functional theory (TDDFT) calculation post-processing, performed with a homemade, freely available, numerical integration code.[17]

Multiple levels of theory were considered, so that the choice of a hybrid or range-separated exchange−correlation functional can be connected to the depicted quantities trends. The influence of solvation was similarly assessed.

2. THEORETICAL BACKGROUND AND COMPUTATIONAL DETAILS

In this section, we detail the theoretical background related to the quantities that will be assessed throughout this survey.

2.1. Original ϕ_S Descriptor. From excited states quantum-chemical calculations, one can compute detachment and attachment density matrices,[14−16] $\mathbf{\Gamma}$ and $\mathbf{\Lambda}$. Related densities, namely, ϱ_Γ and ϱ_Λ, can be integrated through the three dimensions of space to give the ϑ_τ function

$$\vartheta_\tau = \int_{\mathbb{R}} d\xi_1 \int_{\mathbb{R}} d\xi_2 \int_{\mathbb{R}} d\xi_3 \varrho_\tau(\xi_1, \xi_2, \xi_3) \equiv \int_{\mathbb{R}^3} d^3\xi \varrho_\tau(\xi) \quad \tau \equiv \Gamma, \Lambda \tag{1}$$

We can further define a dimensionless ϕ_S index[16] as the overlap between the attachment and detachment densities

$$\phi_S = \vartheta^{-1} \int_{\mathbb{R}^3} d^3\xi \sqrt{\varrho_\Gamma(\xi)\varrho_\Lambda(\xi)}$$
$$\vartheta \equiv \frac{1}{2}\left[\int_{\mathbb{R}^3} d^3\xi \sum_{\tau=\Gamma,\Lambda} \varrho_\tau(\xi)\right] \quad \phi_S \in [0; 1] \tag{2}$$

The ϕ_S index takes values ranging from 0 to 1, depending on the charge-transfer character of the electronic transition. The lowest bound value appears when there is strictly no overlap between detachment and attachment densities, while the highest bound value is obtained in the extreme case where the transition results in a zero photoinduced electronic density fluctuation. Considering these elements, the ϕ_S descriptor can be regarded as a quantitative topological approach to discriminate charge-transfers and valence electronic transitions.

Practically, one usually considers a tridimensional integration grid surrounding the chromophore. The detachment/attachment densities can therefore be integrated over the delimited volume Ω as displayed in the top of Figure 1.

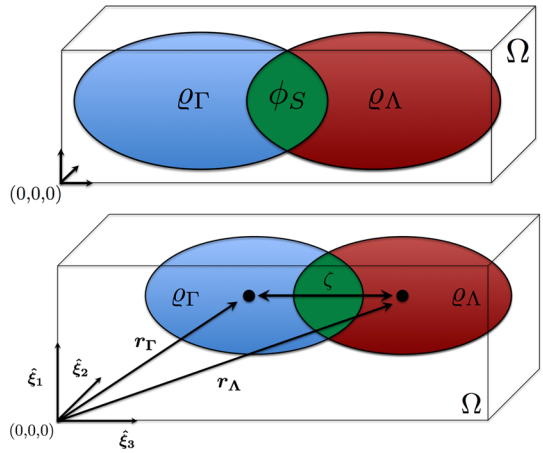

Figure 1. Graphical depiction of the ϕ_S descriptor as the overlap between detachment and attachment densities (top). Computation of detachment/attachment densities centroids (bottom).

2.2. Centroid of Charge Density Variation. As recalled in the Introduction section, in the case of quasi-linear donor−π−acceptor chromophores, it can be interesting to quantify the charge-transfer distance to establish how efficient the photoinduced charge-separation is. Indeed such an information is complementary to the ϕ_S descriptor and of high importance for assessing the push−pull property of a photoactive compound. A possible way to obtain this parameter is to compute the detachment and attachment centroids radius vectors and to calculate the distance between them. Detachment/attachment density centroid coordinates ξ_i^τ with i = 1, 2, 3 (representing x, y, and z, respectively) can be derived by integrating the product of each coordinate value and the target density (ϱ_Γ or ϱ_Λ) over the whole volume

$$\xi_i^\tau = \vartheta_\tau^{-1} \int_{\mathbb{R}^3} d^3\xi \varrho_\tau(\xi)\xi_i \quad i = 1, 2, 3 \quad \tau \equiv \Gamma, \Lambda \tag{3}$$

The centroid radius vectors norm r_τ and the intercentroid distance ζ are defined as follows

dx.doi.org/10.1021/ct500400s | J. Chem. Theory Comput. 2014, 10, 3906−3914

$$r_\tau = \left\{\sum_{i=1}^{3} (\xi_i^\tau)^2\right\}^{1/2} \quad \zeta = \left\{\sum_{i=1}^{3} (\xi_i^\Lambda - \xi_i^\Gamma)^2\right\}^{1/2}$$
$$\tau \equiv \Gamma, \Lambda \tag{4}$$

A graphical depiction of our method is given in the bottom of Figure 1. Note that in general the greater the ζ is the higher the charge-transfer character of a given chromophore is.

Another possibility is to obtain the transferred charge[10−13] by computing the charge density variation ϱ_Δ between the excited ϱ_X and ground ϱ_0 states electron density in the direct space. We define the ϱ_Δ, ϱ_+, and ϱ_- functions as

$$\varrho_\Delta(\xi) = \varrho_X(\xi) - \varrho_0(\xi) \quad \varrho_\pm(\xi) = \frac{1}{2}\left(\sqrt{\varrho_\Delta^2(\xi)} \pm \varrho_\Delta(\xi)\right) \tag{5}$$

The amount of transferred charge χ can be computed, as well as the centroid coordinates

$$\chi_\omega = \int_{\mathbb{R}^3} d^3\xi \varrho_\omega(\xi) \Rightarrow \chi = \frac{1}{2}\sum_{\omega=+,-} \chi_\omega;$$
$$\xi_i^\omega = \chi_\omega^{-1} \int_{\mathbb{R}^3} d^3\xi \varrho_\omega(\xi)\xi_i \quad i = 1, 2, 3 \tag{6}$$

where ω stands for "+" or "−", depending on the density variation function considered. The centroid radius vectors r_ω and the intercentroid distance $\zeta_\pm$ are therefore

$$r_\omega = \left\{\sum_{i=1}^{3} (\xi_i^\omega)^2\right\}^{1/2} \quad \zeta_\pm = \left\{\sum_{i=1}^{3} (\xi_i^+ - \xi_i^-)^2\right\}^{1/2} \tag{7}$$

Note that χ and $\zeta_\pm$ indices defined above correspond to the q_{CT} and D_{CT} ones in eq 10.

Alternatively, detachment/attachment densities instead of density difference can also be used to assess such quantities following similar protocol

$$\tilde{\varrho}_\Delta(\xi) = \varrho_\Lambda(\xi) - \varrho_\Gamma(\xi) \quad \tilde{\varrho}_\pm(\xi) = \frac{1}{2}\left(\sqrt{\tilde{\varrho}_\Delta^2(\xi)} \pm \tilde{\varrho}_\Delta(\xi)\right) \tag{8}$$

where the "∼" symbol stands for detachment/attachment derivation of ϱ_Δ. Because

$$\mathbf{\Delta} = \mathbf{P}_X - \mathbf{P}_0 = \mathbf{\Lambda} - \mathbf{\Gamma} \Rightarrow \varrho_\Delta(\xi) \equiv \tilde{\varrho}_\Delta(\xi) \quad \forall\ \xi \tag{9}$$

we can demonstrate that $\varrho_\omega(\xi) = \tilde{\varrho}_\omega(\xi)$, hence leading to $\chi_\omega = \tilde{\chi}_\omega$. This actually implies

$$\chi \equiv \tilde{\chi} = \frac{1}{2}\sum_{\omega=+,-} \tilde{\chi}_\omega; \quad \xi_i^\omega = \tilde{\xi}_i^\omega \Rightarrow \zeta_\pm = \tilde{\zeta}_\pm \tag{10}$$

so that the intercentroid distance derived by GS/ES density variation or by the difference between detachment and attachment density will be identical. We previously demonstrated[16] that detachment/attachment density matrices can be derived from natural transition orbitals[18−29] density matrices

$$\hat{\gamma}(\mathbf{x}_1, \mathbf{x}_1') \rightarrow \{\mathbf{\Gamma}^{NTO}, \mathbf{\Lambda}^{NTO}\} \leftrightarrow \{\mathbf{\Gamma}, \mathbf{\Lambda}\} \leftarrow \hat{p}_y = |\Psi_y\rangle\langle\Psi_y| \tag{11}$$

where $\hat{\gamma}(x_1, x_1')$ is the *one-particle reduced transition density projector*, and y can correspond either to 0 for the ground state projector or to X for the excited state projector. We can therefore conclude that

$$\phi_S^{NTO} = \phi_S \Leftarrow \mathbf{\Lambda}^{NTO} - \mathbf{\Gamma}^{NTO} = \mathbf{\Lambda} - \mathbf{\Gamma}$$
$$\tilde{\chi}_\omega^{NTO} = \tilde{\chi}_\omega \Rightarrow \tilde{\zeta}_\pm^{NTO} = \tilde{\zeta}_\pm \tag{12}$$

This implies that topological quantities can be similarly obtained from the two different operators. The last statement will be numerically validated in the Results section.

At this point, we wish to point out that the value of $\zeta_\pm$ ($\tilde{\zeta}_\pm$) will be rather different from the ζ computed from the total detachment and attachment densities. Indeed, because in the case of $\zeta_\pm$ ($\tilde{\zeta}_\pm$) only differences of densities in the direct space were involved, if any overlap between GS/ES (or detachment/attachment) densities occurs, then the fraction of overlapping density will be canceled by the difference in eq 5 and hence will not be accounted for in the computation of the intercentroid distance. This leads to different values for the computed quantities. By construction, $\tilde{\zeta}_\pm$ ($\zeta_\pm$) will take values greater or equal to ζ. This phenomenon can be graphically explained as in Figure 2, where we presented the variation δ_ω in the evaluation of r_ω by using density differences (eq 10) with respect to the computation of detachment/attachment centroids (eq 7).

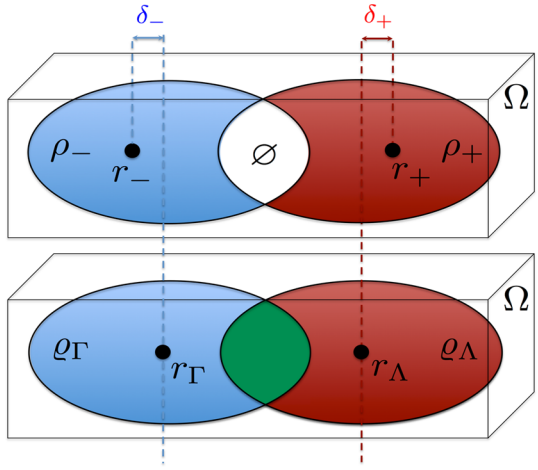

Figure 2. Two definitions of the intercentroid distance by the use of direct (top) and Hilbert (bottom) space preliminary operations. Note that in the top image, densities variations ρ_ω can equivalently correspond to ϱ_ω or $\tilde{\varrho}_\omega$.

Moreover, if two acceptors are disposed symmetrically around a single donor, even a long-range charge-transfer transition will result in detachment and attachment centroid radius vectors located at the center of the molecule and hence will lead to a zero charge-transfer distance even for a charge-transfer transition, as displayed in Figure 3. This problem still holds when there is no central donor (see the *n*III-b and *n*VI-b molecular set) or in the case of symmetrical homoleptic inorganic complexes for which the target transition is a metal-

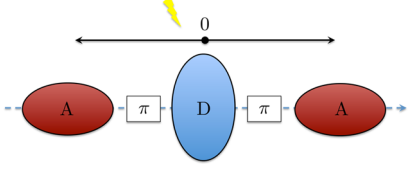

Figure 3. Zero detachment/attachment radius vectors in the case of linear symmetric donor−π−acceptor chromophore.

dx.doi.org/10.1021/ct500400s | J. Chem. Theory Comput. 2014, 10, 3906−3914

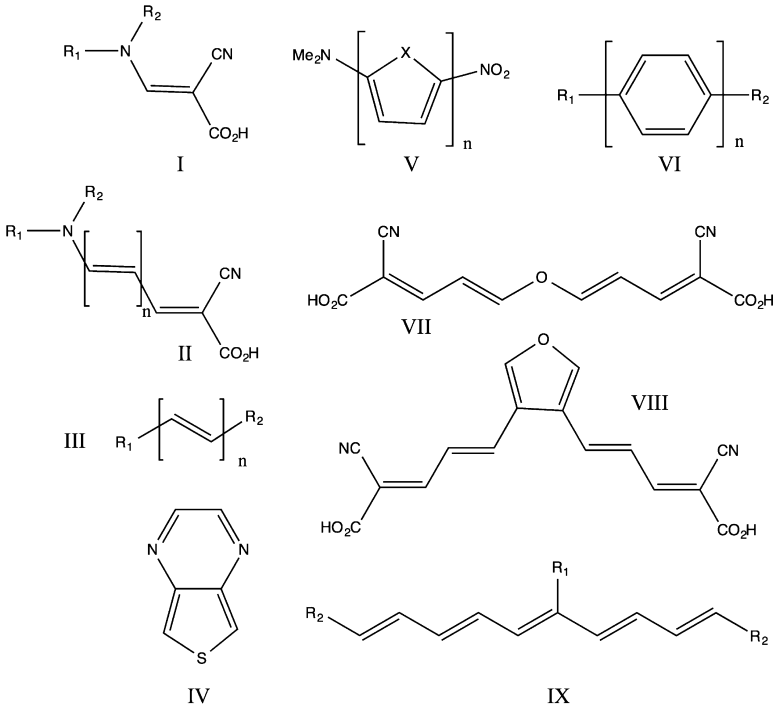

I-(a,b)	R_1=R_2=(H,Me)	nII-(a,b)	R_1=R_2=(H,Me), n=(1,5)
nIII-(a,b)	R_1=R_2=(NMe_2,NO_2), n=(1,5)	nIII-(c,d)	R_1=(NH_2,NMe_2),R_2=NO_2, n=(1,5)
IV-n	n=(1,36)	nV-X	X=(NH,O,S,Se), n=(1,5)
nVI-(a,b)	R_1=R_2=(NMe_2,NO_2), n=(1,5)	nVI-c	R_1=NMe_2, R_2=NO_2, n=(1,5)
IX-a	R_1=NO_2,R_2=NMe_2	IX-b	R_1=NMe_2,R_2=NO_2

Figure 4. Sketch of the molecules investigated in the present survey.

to-ligand charge-transfer that reorganizes the electron density from the central metal toward the ligands. This constitutes a limitation of the barycenter strategy usage that can be overcome by considering the computation of the displaced charge together with the assessment of the detachment/attachment densities overlap (ϕ_S index).

2.3. Computational Strategy. The molecular systems involved in this survey are presented in Figure 4. Those are mostly π-conjugated sensitizers with the general structure donor−bridge−acceptor (D−π−A) dyes. They were chosen because they are known to exhibit low-energy light absorption and consequent intramolecular charge-transfer.

Among the sensitizers depicted in Figure 4, we find a set of α,ω-NMe_2,NO_2 molecules,[30,31] with donor−acceptor fragments spaced by double bonds (III dyes), phenyles (VI dyes), thiophenes, pyrroles, furanes, or selenophenes (*n*V-X dyes). The number *n* of spacer subunits takes values from 1 to 5 for each of the molecular subsets.

We also considered some dyes constituted by two donor (acceptor) groups separated by double bonds or phenyles spacers. Those are known as push−push (respectively, pull−pull) chromophores.

The IV[th] subset of molecules consists in a set of 36 thieno[3,4-*b*]pyrazines derivatives and was previously studied by Jacquemin et al.[13] with the help of the barycenter approach with second-order excited states electron densities. These molecules will be used for the computation of the amount of transferred charge from detachment/attachment densities according to the two possible derivations (from excited/ground state density matrices difference and from virtual/occupied natural transition orbitals density matrices difference) because they are expected to provide equivalent results with linear-response excited states electron densities.

All the sensitizers' ground state geometry and transition energies were computed with the DFT and linear-response TDDFT methods. All the calculations were performed using Gaussian 09 (revision B01) package.[32] The first set of molecules (Figure 4, except the IV derivatives) geometries were computed using the PBE0/6-311G(d,p) level of theory[33−35] with tight convergence criteria imposed both on the self-consistent field (residual mean square is 10^{-9} a.u.) and on geometry optimization (residual mean square force threshold is 10^{-5} a.u.). This protocol is chosen because it is known to provide reliable geometries for organic compounds. Frequency calculations were further performed on these equilibrium geometries with the same level of theory to confirm that the optimized geometries are true minima of the potential energy surface. Excited states were computed considering the Franck−Condon principle stating that all the electronic excitations are vertical. Various exchange−correlation functionals were used, namely, the parameter-free PBE0, hybrid B3LYP,[36,37], and range-separated CAM-B3LYP[38] xc-functionals together with the 6-311++G(2d,p) basis set[35] (except for the IV subset, see below). This choice of functionals allows us to draw some comparisons related to the use of different hybrid functionals or the comparison between a hybrid functional and its long-range corrected version. Barycenter-related indices are computed from detachment/attachment densities. The sensi-

dx.doi.org/10.1021/ct500400s | J. Chem. Theory Comput. 2014, 10, 3906−3914

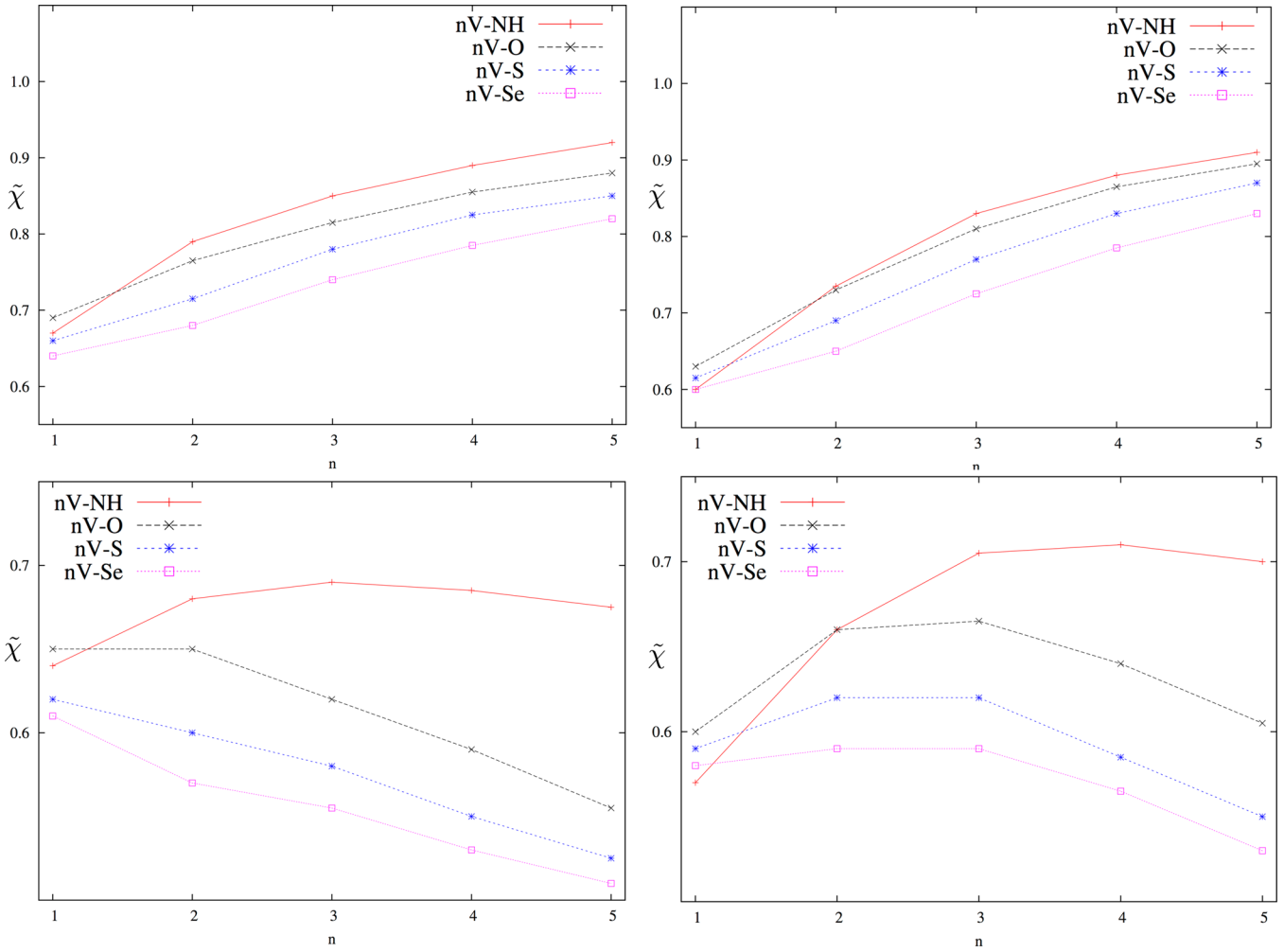

Figure 5. $\tilde{\chi}$ values (in atomic units of charge) with respect to the number of spacer subunits (nV-X subset) computed with B3LYP (top) and CAM-B3LYP (bottom) in vacuum (left) and acetonitrile (right).

tizers structural and optical properties were computed in vacuum and in acetonitrile (except for the IV derivatives). Acetonitrile solvation effects were taken into account using of a self-consistent reaction field[39] (SCRF) thanks to the integral equation formalism[40,41] (IEF) of the polarizable continuum model[39] (PCM).

Molecules belonging to the IV set were computed with the level of theory reported in a previous study,[13] i.e., PBE0/6-311G(d,p) for geometry optimization and CAM-B3LYP/6-311+G(2d,p) for excited states computation. Acetonitrile solvation effects were also modeled by IEF−PCM. Again, frequency calculations ensured that no transition state was computed. Six electronic transitions were calculated for each of these molecules, and natural transition orbitals as well as detachment/attachment density matrices were obtained. The topological parameters were computed for the six transitions of each molecule of the IV set.

All the detachment/attachment densities, natural transition orbitals, ϕ_S, density barycenters, transferred charges, and charge-transfer distances were computed using a homemade (freely distributed) code developed in our laboratory.[17]

3. RESULTS

Results related to the molecules from Figure 4 (absorption wavelengths and respective oscillator strengths, ϕ_S, and centroid-related indices) are reported in the Supporting Informations. As we expected, because B3LYP and PBE0 (which unsurprisingly give very close results) are known to systematically overestimate the charge-transfer, $\tilde{\chi}$, $\tilde{\zeta}_{\pm}$, and ζ values are higher with these hybrid functionals than with CAM-B3LYP. We notice that in the case of push−pull dyes, $\tilde{\zeta}_{\pm}$ and ζ fluctuation magnitude between B3LYP (PBE0) and CAM-B3LYP is more important than the $\tilde{\chi}$ fluctuation. Furthermore, while an increase in the spacer size extension induces an important rise of barycenter-related indices values with B3LYP (PBE0), CAM-B3LYP shows a much lower sensitivity to the number of spacer subunits. One can notice that, as expected, higher ϕ_S values are observed when $\tilde{\chi}$, $\tilde{\zeta}_{\pm}$, and ζ values are low.

The contribution of the solvation is noticeable. The barycenter-related quantity values are higher in vacuum than in acetonitrile. This appears to be consistent with the fact that the ϕ_S index is systematically slightly lower in acetonitrile than in vacuum. The $\tilde{\chi}$ and ζ trends for the nV-X subset computed with B3LYP and CAM-B3LYP in vacuum and acetonitrile are displayed in Figures 5 and 6, respectively. The CAM-B3LYP results appear to be in perfect agreement with the trends reported by Ciofini et al. in ref 30, i.e., the $\tilde{\chi}$ and ζ values increase until they reach a maximum for a given number of spacer subunits before decreasing until n = 5.

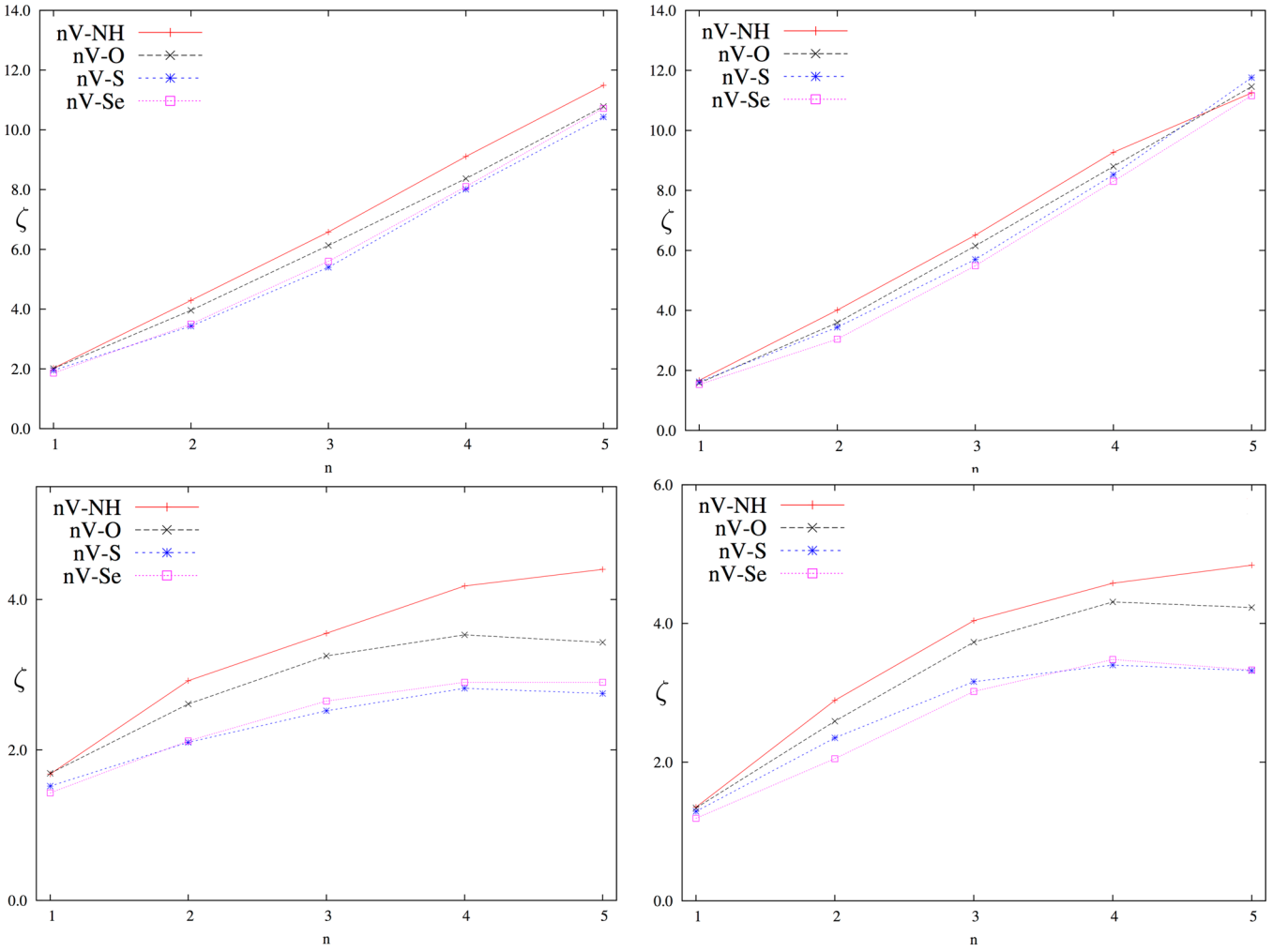

Figure 6. ζ values (in Å) with respect to the number of spacer subunits (nV-X subset) computed with B3LYP (top) and CAM-B3LYP (bottom) in vacuum (left) and acetonitrile (right).

One might note that the nIII-a (the push−push dye with oligoene spacer) ϕ_S index values are systematically much lower than those of nIII-b. Conversely, switching from a push−push (IX-a) to a pull−pull (IX-b) dye with a central branched group makes the ϕ_S descriptor value systematically drop by more than 10%. We can therefore conclude that the presence of a central acceptor (respectively, donor) branched to the push−push (pull−pull) chromophore with an oligoene spacer (IX-a,b) completely reverses the behavior of ϕ_S with respect to the bare push−push (pull−pull) dyes with oligoene spacers (nIII-a,b).

It is worth noting that the ϕ_S index values are higher for the nII-b molecules than for the nIII-d ones, denoting a higher electron-withdrawing ability of the nitro group with respect to the cyanoacrylic acceptor.

We also noticed that switching the central donor of VII from a simple ether to a furane does not have a strong impact on the detachment/attachment overlap as expected.

Interestingly, the nIII-b (pull−pull dye with oligoene spacers) and nVI-b (pull−pull with phenyl spacers) subsets exhibit zero intercentroid distances and zero detachment/attachment centroid radius vectors. The simple fact to put the two acceptor groups symmetrically causes $\tilde{\zeta}_{\pm}$ and ζ to vanish despite the fact that a nonzero amount of charge is transferred through the electronic transition. The model case sketched in Figure 4 is therefore particularly well illustrated by the nIII-b molecular subset (though no central donor is grafted to the molecule) and is graphically illustrated in Figure 7 with the 5III-b molecule's detachment and attachment densities plot.

An interesting case is the 5VI-c molecule's first transition that constitutes a paradigmatic case of charge-transfer. We present its detachment/attachment density plots on the left part of Figure 8. With the PBE0 functional in acetonitrile, the ϕ_S index

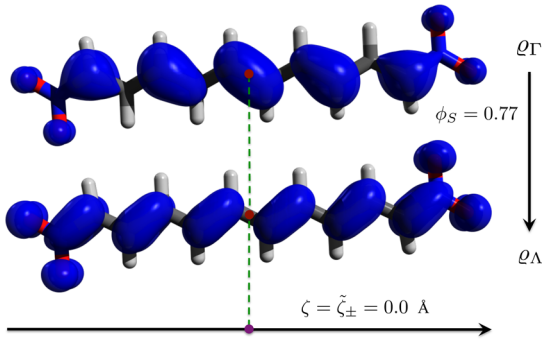

Figure 7. 5III-b molecule detachment/attachment densities and centroids plots and, obtained with PCM−PBE0/6-311+G(2d,p) level of theory. $\tilde{\zeta}_{\pm}$ and ζ are the intercentroid distances computed from eqs 10 and 7, respectively.

dx.doi.org/10.1021/ct500400s | J. Chem. Theory Comput. 2014, 10, 3906−3914

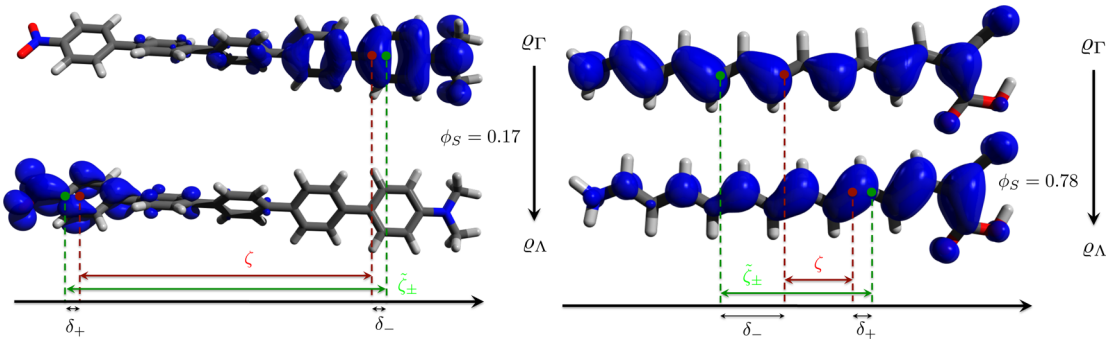

Figure 8. 5VI-c in acetonitrile (left) and 5II-a in vacuum (right). Detachment/attachment densities and centroids plots with PBE0. Difference between ζ and $\tilde{\zeta}_\pm$ is highlighted through $\delta_\pm$ representation. The intercentroid distances, $\tilde{\zeta}_\pm$ and ζ, are computed from eqs 10 and 7, respectively.

value for this molecule is 0.17, which is extremely low. We evidenced on this figure the variation between the intercentroid distance computed from the difference of detachment and attachment densities in direct space ($\tilde{\zeta}_\pm$, eq 10) and from the simple computation of the detachment and attachment densities centroids (ζ, eq 7). This variation, which amounts to 0.77 Å in this case, is much more striking for the 5II-a molecule (i.e., the δ_+ and δ_- values are higher in magnitude) where the difference between $\tilde{\zeta}_\pm$ and ζ is 5.35 Å. This result can be explained by the high calculated value of ϕ_S (0.78), which means (Figure 3) that a large amount of detachment and attachment densities were not accounted in the computation of the intercentroid distance in the case of $\tilde{\zeta}_\pm$. The difference between the intercentroid distance definitions is evidenced in Figure 9 where we plotted $\tilde{\zeta}_\pm$ and ζ values for the *n*V-X set of

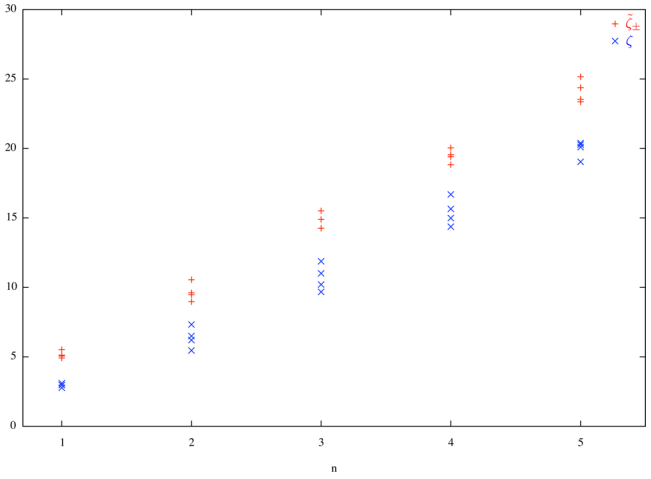

Figure 9. Comparison between the intercentroid distances $\tilde{\zeta}_\pm$ and ζ values (in Å) for the *n*V-X set of chromophores (X═NH,O,S and Se; n = 1−5) computed with PBE0 in acetonitrile.

molecules (X═NH,O,S and Se; n = 1−5) in acetonitrile (the PBE0 xc-functional was used here to highlight the trends because the magnitude of the intercentroid distance values fluctuation is higher with an hybrid functional, see ref 16). We clearly see here that all the values of $\tilde{\zeta}_\pm$ are systematically higher than those of ζ, which confirms our hypothesis.

In Figure 10, we present the ϕ_S values as a function of $\tilde{\chi}$ for the *n*V-X, II-a,b, and VI-c sets of molecules with all the levels of theory used throughout this paper. A quadratic relationship is evidence, although some dispersion of the value is present. Although this trend is very qualitative, it appears that the ϕ_S

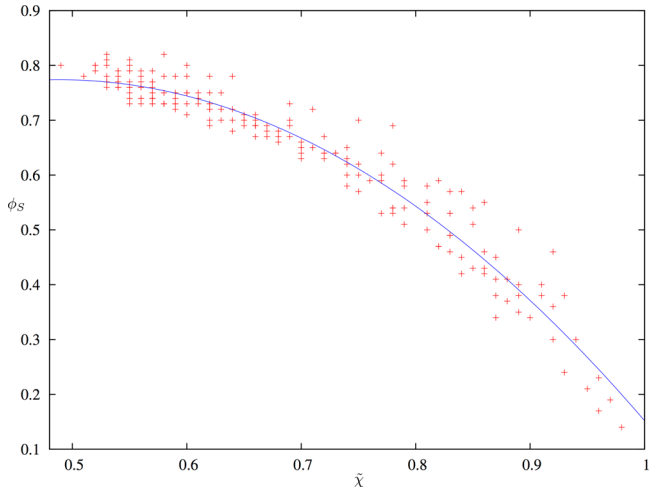

Figure 10. Quadratic-like relationship between ϕ_S and the amount of transferred charge ($\tilde{\chi}$) values for *n*V-X, II-a,b, and *n*VI-c compounds from the present study.

descriptor value dramatically drops when the amount of transferred charge increases. This behavior is clearly expected because a high value of transferred charge means that the overlap between detachment and attachment must be low because it actually corresponds to a charge-transfer. This result highlights the complementarity between the two approaches.

From the computation of the IV-derivatives excited states, we could highlight (Supporting Informations) the perfect equivalence between barycenter-related indices derived from detachment/attachment densities obtained from the $\hat{\gamma}(x_1, x_1')$ and the $|\Psi_y\rangle\langle\Psi_y|$ projectors (identity relationships with all R^2 equal to 1.000), which is in perfect agreement with our theoretical deductions.

4. CONCLUSION

The mathematical background of the barycenter approach has been recalled, and we could demonstrate that the quantities related to this approach can be computed both with excited/ground state densities or with detachment/attachment densities. We further exposed the hypothetical problems that could be encountered through the use of such a topological approach and the possible solutions that could be brought by our new method. The computation of topological parameters has been done for a large set of molecules (push−push, push−pull, and pull−pull, for instance) and has been performed within various levels of theories. Both approaches allow us to evidence the behavior of an exchange−correlation functional

with respect to the charge-transfer character of a chromophore. From these results, we could clearly evidence similarities and discrepancies between our new approach and the formerly developed descriptors. It especially appeared that both models can be useful (with some formally exposed and validated complementarity) for deducing some crucial data from the computation of electronic transitions of target sensitizers that can potentially be used for dye-sensitized solar cells (donor−π−acceptor dyes) for instance. Some critical points of the barycenter approach could be evidenced, such as the different definition of the intercentroid distance from direct space integration and the zero interbarycenter distance for molecules of symmetric constitution. The connection between this approach and the ϕ_S descriptor through a quadratic-like relationship could be qualitatively established. Finally, a third possible derivation of the barycenter descriptors from natural transition orbitals was suggested and numerically validated by quantum chemical calculations.

■ ASSOCIATED CONTENT

Supporting Information

Transition wavelength, oscillator strength, charge-transfer and barycenter-related indices,and ϕ_S index values with PBE0, B3LYP, and CAM-B3LYP in vacuum and acetonitrile. Charge-transfer and ϕ_S index values from detachment/attachment and NTOs density matrices. This material is available free of charge via the Internet at http://pubs.acs.org.

■ AUTHOR INFORMATION

Corresponding Author

*E-mail: thibaud.etienne@univ-lorraine.fr.

Notes

The authors declare no competing financial interest.

■ ACKNOWLEDGMENTS

A.M. thanks CNRS for funding the "chaire d'excellence" project. All the authors are very grateful to the PhiScience Association for its valuable activity. Dr. Thibaut Very is acknowledged for his contribution to the development of the NANCY_EX software suite. We also acknowledge support from the "Balance Supra" ANR project.

■ REFERENCES

(1) Labat, F.; Le Bahers, T.; Ciofini, I.; Adamo, C. First-principles modeling of dye-sensitized solar cells: Challenges and perspectives. *Acc. Chem. Res.* **2012**, *45*, 1268−1277.

(2) Le Bahers, T.; Pauporté, T.; Lainé, P. P.; Labat, F.; Adamo, C.; Ciofini, I. Modeling dye-sensitized solar cells: From theory to experiment. *J. Phys. Chem. Lett.* **2013**, *4*, 1044−1050.

(3) Hagfeldt, A.; Grätzel, M. Molecular photovoltaics. *Acc. Chem. Res.* **2000**, *33*, 269−277.

(4) Preat, J.; Hagfeldt, A.; Perpète, E. A. Investigation of the photoinduced electron injection processes for p-type triphenylamine-sensitized solar cells. *Energy Environ. Sci.* **2011**, *4*, 4537−4549.

(5) Etienne, T.; Chbibi, L.; Michaux, C.; Perpète, E. A.; Assfeld, X.; Monari, A. All-organic chromophores for dye-sensitized solar cells: A theoretical study on aggregation. *Dyes Pigm.* **2014**, *101*, 203−211.

(6) Preat, J.; Michaux, C.; Jacquemin, D.; Perpète, E. A. Enhanced efficiency of organic dye-sensitized solar cells: Triphenylamine derivatives. *J. Phys. Chem. C* **2009**, *113*, 16821−16833.

(7) Tang, J.; Qu, S.; Hu, J.; Wu, W.; Hua, J. A new organic dye bearing aldehyde electron-withdrawing group for dye-sensitized solar cell. *Sol. Energy* **2012**, *86*, 2306−2311.

(8) Guido, C. A.; Cortona, P.; Mennucci, B.; Adamo, C. On the metric of charge transfer molecular excitations: A simple chemical descriptor. *J. Chem. Theory Comput.* **2013**, *9*, 3118−3126.

(9) Guido, C. A.; Cortona, P.; Adamo, C. Effective electron displacements: A tool for time-dependent density functional theory computational spectroscopy. *J. Chem. Phys.* **2014**, *140*, 104101.

(10) Le Bahers, T.; Adamo, C.; Ciofini, I. A qualitative index of spatial extent in charge-transfer excitations. *J. Chem. Theory Comput.* **2011**, *7*, 2498−2506.

(11) Garcia, G.; Adamo, C.; Ciofini, I. Evaluating push−pull dye efficiency using TD-DFT and charge transfer indices. *Phys. Chem. Chem. Phys.* **2013**, *15*, 20210−20219.

(12) Jacquemin, D.; Le Bahers, T.; Adamo, C.; Ciofini, I. What is the "best" atomic charge model to describe through-space charge-transfer excitations? *Phys. Chem. Chem. Phys.* **2012**, *14*, 5383−5388.

(13) Céron-Carrasco, J. P.; Siard, A.; Jacquemin, D. Spectral signatures of thieno[3,4-b]pyrazines: Theoretical interpretations and design of improved structures. *Dyes Pigm.* **2013**, *99*, 972−978.

(14) Monari, A.; Assfeld, X.; Beley, M.; Gros, P. C. Theoretical study of new ruthenium-based dyes for dye-sensitized solar cells. *J. Phys. Chem. A* **2011**, *115*, 3596−3603.

(15) Dreuw, A.; Head-Gordon, M. Single-reference ab initio methods for the calculation of excited states of large molecules. *Chem. Rev.* **2005**, *105*, 4009−4037.

(16) Etienne, T.; Assfeld, X.; Monari, A. Toward a quantitative assessment of electronic transitions' charge-transfer character. *J. Chem. Theory Comput.* **2014**, DOI: 10.1021/ct5003994.

(17) NAncy-EX. http://nancyex.sourceforge.net (accessed June 13, 2014).

(18) Luzanov, A. V.; Sukhorukov, A. A.; Umanskii, V. É. Application of transition density matrix for analysis of excited states. *Theor. Exp. Chem.* **1976**, *10*, 354−361.

(19) Martin, R. L. Natural transition orbitals. *J. Chem. Phys.* **2003**, *118*, 4775−4777.

(20) Batista, E. R.; Martin, R. L. Natural Transition Orbitals. In *Encyclopedia of Computational Chemistry*; John Wiley & Sons, Ltd.: New York, 2004.

(21) Mayer, I. Using singular value decomposition for a compact presentation and improved interpretation of the CIS wave functions. *Chem. Phys. Lett.* **2007**, *437*, 284−286.

(22) Mayer, I. Identifying a pair of interacting chromophores by using SVD transformed CIS wave functions. *Chem. Phys. Lett.* **2007**, *443*, 420−425.

(23) Very, T.; Despax, S.; Hébraud, P.; Monari, A.; Assfeld, X. Spectral properties of polypyridyl ruthenium complexes intercalated in DNA: Theoretical insights into the surrounding effects of [Ru(dppz)-(bpy)2]2+. *Phys. Chem. Chem. Phys.* **2012**, *14*, 12496−12504.

(24) Chantzis, A.; Very, T.; Daniel, C.; Monari, A.; Assfeld, X. Theoretical evidence of photo-induced charge transfer from DNA to intercalated ruthenium (II) organometallic complexes. *Chem. Phys. Lett.* **2013**, *578*, 133−137.

(25) Lachaud, F.; Jeandon, C.; Monari, A.; Assfeld, X.; Beley, M.; Ruppert, R.; Gros, P. C. New dyads using (metallo)porphyrins as ancillary ligands in polypyridine ruthenium complexes. Synthesis and electronic properties. *Dalton Trans.* **2012**, *41*, 12865−12871.

(26) Chantzis, A.; Very, T.; Monari, A.; Assfeld, X. Improved treatment of surrounding effects: UV/vis absorption properties of a solvated Ru(II) complex. *J. Chem. Theory Comput.* **2012**, *8*, 1536−1541.

(27) Lachaud, F.; Jeandon, C.; Beley, M.; Ruppert, R.; Gros, P. C.; Monari, A.; Assfeld, X. Ground and excited state properties of new porphyrin based dyads: A combined theoretical and experimental study. *J. Phys. Chem. A* **2012**, *116*, 10736−10744.

(28) Monari, A.; Very, T.; Rivail, J.-L.; Assfeld, X. A QM/MM study on the spinach plastocyanin: Redox properties and absorption spectra. *Comput. Theor. Chem.* **2012**, *990*, 119−125.

(29) Etienne, T.; Michaux, C.; Monari, A.; Assfeld, X.; Perpète, E. A. Theoretical computation of Betain B30 solvatochromism using a polarizable continuum model. *Dyes Pigm.* **2014**, *100*, 24−31.

(30) Ciofini, I.; Le Bahers, T.; Adamo, C.; Odobel, F.; Jacquemin, D. Through-space charge transfer in rod-like molecules: Lessons from theory. *J. Phys. Chem. C* **2012**, *116*, 11946−11955.
(31) Ciofini, I.; Le Bahers, T.; Adamo, C.; Odobel, F.; Jacquemin, D. Correction to "Through-space charge transfer in rod-like molecules: Lessons from theory. *J. Phys. Chem. C* **2012**, *116*, 14736−14736.
(32) Frisch, M. J.; Trucks, G. W.; Schlegel, H. B.; Scuseria, G. E.; Robb, M. A.; Cheeseman, J. R.; Scalmani, G.; Barone, V.; Mennucci, B.; Petersson, G. A.; Nakatsuji, H.; Caricato, M.; Li, X.; Hratchian, H. P.; Izmaylov, A. F.; Bloino, J.; Zheng, G.; Sonnenberg, J. L.; Hada, M.; Ehara, M.; Toyota, K.; Fukuda, R.; Hasegawa, J.; Ishida, M.; Nakajima, T.; Honda, Y.; Kitao, O.; Nakai, H.; Vreven, T.; Montgomery, J. A.; , Jr., Peralta, J. E.; Ogliaro, F.; Bearpark, M.; Heyd, J. J.; Brothers, E.; Kudin, K. N.; Staroverov, V. N.; Keith, T.; Kobayashi, R.; Normand, J.; Raghavachari, K.; Rendell, A.; Burant, J. C.; Iyengar, S. S.; Tomasi, J.; Cossi, M.; Rega, N.; Millam, J. M.; Klene, M.; Knox, J. E.; Cross, J. B.; Bakken, V.; Adamo, C.; Jaramillo, J.; Gomperts, R.; Stratmann, R. E.; Yazyev, O.; Austin, A. J.; Cammi, R.; Pomelli, C.; Ochterski, J. W.; Martin, R. L.; Morokuma, K.; Zakrzewski, V. G.; Voth, G. A.; Salvador, P.; Dannenberg, J. J.; Dapprich, S.; Daniels, A. D.; Farkas, O.; Foresman, J. B.; Ortiz, J. V.; Cioslowski, J.; Fox, D. J. *Gaussian 09*, revision B.01, Gaussian, Inc.: Wallingford, CT, 2010.
(33) Adamo, C.; Barone, V. Toward reliable density functional methods without adjustable parameters: The PBE0 model. *J. Chem. Phys.* **1999**, *110*, 6158−6170.
(34) Adamo, C.; Scuseria, G. E.; Barone, V. Accurate excitation energies from time-dependent density functional theory: Assessing the PBE0 model. *J. Chem. Phys.* **1999**, *111*, 2889−2899.
(35) Frisch, M. J.; Pople, J. A.; Binkley, J. S. Self-consistent molecular orbital methods 25. Supplementary functions for Gaussian basis sets. *J. Chem. Phys.* **1984**, *80*, 3265−3269.
(36) Becke, A. D. Density-functional thermochemistry. III. The role of exact exchange. *J. Chem. Phys.* **1993**, *98*, 5648−5652.
(37) Lee, C.; Yang, W.; Parr, R. G. Development of the Colle−Salvetti correlation-energy formula into a functional of the electron density. *Phys. Rev. B* **1988**, *37*, 785−789.
(38) Yanai, T.; Tew, D. P.; Handy, N. C. A new hybrid exchange-correlation functional using the Coulomb-attenuating method (CAM-B3LYP). *Chem. Phys. Lett.* **2004**, *393*, 51−57.
(39) Tomasi, J.; Mennucci, B.; Cammi, R. Quantum mechanical continuum solvation models. *Chem. Rev.* **2005**, *105*, 2999−3094.
(40) Cancès, E.; Mennucci, B.; Tomasi, J. A new integral equation formalism for the polarizable continuum model: Theoretical background and applications to isotropic and anisotropic dielectrics. *J. Chem. Phys.* **1997**, *107*, 3032−3041.
(41) Mennucci, B.; Cancès, E.; Tomasi, J. Evaluation of solvent effects in isotropic and anisotropic dielectrics and in ionic solutions with a unified integral equation method: Theoretical bases, computational implementation, and numerical applications. *J. Phys. Chem. B* **1997**, *101*, 10506−10517.